

Between Gaming and Microclimate Simulations: Temperature Estimation of an Urban Area

Eva Strauss and Dimitri Bulatov ^a

*Fraunhofer Institute for Optronics, System Technologies and Image Exploitation (IOSB),
Gutleuthausstrasse 1, 76275 Ettlingen, Germany*

Keywords: Urban Heat Island, Thermal Simulation, Digital Twin, 3D City Model, Thermal Remote Sensing.


Abstract: With the rising awareness and interest from researchers, local authorities, and industry in the urban heat island effect, thermal remote sensing data is needed as it allows for identification, tracking, or analysis of land surface temperatures. Yet, the accessibility of appropriate thermal data in both the spatial and temporal domain states an inhibiting factor. Whilst thermal satellite data suffers from both low spatial and temporal resolution, airborne imagery might enable adequate resolutions, however, is not acquired without time and cost consumption. One way to overcome this drawback is the generation of synthetic data, which comprises the simulation of surface temperatures. These rather simplified simulations are either quite fast, as desired in gaming applications, however, highly inaccurate, or rather complex, holistic, time-consuming and computationally intensive, like applied in urban microclimate considerations. In this paper, we present an in-between approach towards the estimation of urban surface temperatures that aims to fill this gap between holistic microclimate simulations and climate maps.

1 INTRODUCTION

1.1 Motivation

In the last century, the world-wide urbanization degree increased tremendously, and by 2050, the portion of people living in cities or urbanized areas is expected to be almost 70%. With the concurrent increase of summer heat periods, researcher, local authorities and industry became aware of the need to maintain the city as a livable area by taking countermeasures against the so-called urban heat island (UHI) effect. This effect describes the overall higher temperatures of urban areas compared to their rural surroundings. Its cause is found in cityscapes, construction materials and type, latent factors like population density or traffic, and others. Therefore, many countermeasures currently applied or under research evolve around these causes, and interest in computer-aided tools to quantify the actual effect of countermeasures is growing. One such computer-aided tool is given by urban climate simulation software. There, heat transport and flow dynamics are usually considered, which makes the overall simulation a complex,

time-consuming task requiring interdisciplinary expert knowledge. Thus, it is not feasible for, e.g., architects or urban planners who seek rather fast and easy to generate as well easy to interpret results. Looking for a faster way to simulate the temperature distribution of an urban area, one might look into the area of gaming and physics-based sensor simulations. Here, simulation runtimes are drastically reduced up to realtime, however, stream dynamics are not taken into account. In other words, the flow and temperature of air through a city, its convective cooling and its effect on human comfort, which is generally of essence, are not considered. Last but not least, climate maps state another very fast option to estimate local urban climate. No differential equations need to be numerically solved, instead, urban areas are segmented by their local climate solely depending on land-use, vertical roughness, topography, portion of water bodies, and similar features. In summary, a large gap in accuracy between near real-time climate estimations and holistic micro-climate simulations can be identified by the urban planners. To bridge the gap, a tool for a quick, superficial screening of a large urban scene is required allowing to detect potential areas of urban heat accumulation. For a few candidates of (smaller) areas particularly vulnerable to UHIs, a

^a  <https://orcid.org/0000-0002-0560-2591>

comprehensive micro-climate simulation can be then launched, thus allowing to save time and computational resources. In this paper, we present an in-between approach towards surface temperature simulation serving as previously mentioned tool. We particularly address the physical modeling of the heat transfer. Thus in this context, the proposed methods are more sophisticated than gaming approaches, yet significantly simplified in direct comparison to micro-climate simulations.

The rest of the paper is organized as follows: To systematize the state of the art on available tools on thermal simulation, we provide a concise overview of current simulation methods and software in Section 1.2 and an introduction to the base simulation framework we built up on in Section 2.1. Afterwards, we present our methods of choice in Section 2, which is followed by the evaluation of our methods in Section 3. Finally, we summarize our findings and future work in Section 4.

1.2 Related Work

While the UHI describes temperature increase of cities in comparison to their rural surrounding, the microclimate generally refers to the ground-level climate influenced by the physical characteristics of the present surfaces. An alternative to laborious and costly inner-city measurements is provided by micro-climate simulations. They make it possible to cover large areas, analyze the impact of city design on UHI formation and even thermal comfort. One quite well-known commercial software for microclimate simulations is ENVI-met (Liu et al., 2021). This tool allows for simulation of single building (yet no interior), city quarters or whole smaller cities. Designed as a holistic approach, each physical phenomenon influencing the microclimate is modeled, including radiative heat exchange, photosynthesis, and evapotranspiration. Another simulation tool under ongoing development is PALM-4U. As research project under national funding by the German Federal Ministry of Education and Research (BMBF), the open-source software is designed to help in municipal adaptation strategies concerning the UHI and other climate-related changes in urban areas. It offers a higher resolution in turbulences and is highly parallelized. With PALM-4U, it is aimed for usability in civil service and public authority. Envi-met and PALM-4U, as usual microclimate simulation tools, are based on continuous fluid dynamics (CFD) to numerically solve for the temperature and wind fields. They provide great accuracy, yet by their CFD nature, they are time-consuming and demanding, require expertise in the field of numerical

simulation and thus specific training.

Other simulations frameworks focus on specific tasks or reduced scale, such as building energy tools for single building simulation. They provide great detail on an appropriate scale, yet cannot be extended to the urban city scale without huge drawbacks in computation time and cost. Thus, to overcome the gap between precise building energy simulation (BES) and CFD on urban areas, BES-CFD coupling techniques have been researched (Rodríguez-Vázquez, Martín and Hernández-Pérez, Iván and Xamán, Jesus and Chávez, Yvonne and Gijón-Rivera, Miguel and Belman-Flores, Juan M., 2020; Ruijun Zhang, 2021). Bringing together the respective advantages, high computation time and cost still remains.

Shifting the point of view from microclimate simulation tools towards scene generation and more game oriented tools, such as the software components by Presagis (Presagis, 2023) or Oktal-SE (Oktal-SE, 2023), a paradigm change can be observed. Instead of expensive CFD simulation, these tools mostly rely on highly simplified surface temperature simulation and rather focus sophisticated camera models. Thus, they clearly outperform microclimate simulations in terms of runtime and computational cost, yet to the extent of accuracy.

Motivated and inspired from the above methodologies to urban temperatures, our approach aims at converging these by picking and combining respective models and thus yielding reliable results with appropriate computation time, cost, and accuracy.

2 METHODOLOGY

2.1 Preliminaries

The heat distribution of an urban area depends on many factors, which makes its computation a challenging task. These factors include, but are not limited to: construction materials and geometries, climate conditions (both macro- and micro-climate), local weather conditions and weather history over a larger time span, as well as factors depending on the residents, like population or traffic. Each of these contributes to the generation or transfer of heat and raises the need for a huge amount of information given prior to climate simulations. A so-called digital twin, which combines 3D geometry with additional information, states a great starting point for urban temperature estimation. In this paper, we focus on the cityscape and construction materials, and refer to the digital twin as the 3D reconstruction of an urban area, in form of a triangle mesh, with semantic

and material information. Since the aerial data provide the most cost-efficient method to derive the most essential information from large scene, we followed the procedure of (Bulatov et al., 2020) to generate the digital twin from a high-resolution orthophoto, a normalized digital surface model (ndsm), multi-spectral imagery, and OSM data. In a nutshell, an index is assigned by semantic segmentation and material classification to each triangle representing its semantic type (ground, building part or vegetation), its material type (i.e. street, grass, soil, or water for ground triangles, roof or wall for buildings, and forest, deciduous tree, shrub or palm tree for vegetation), as well as color (image-derived for visible and geo-typical for non-visible, such as building walls, objects). These indices are linked to a material database where physical parameters like density, heat conductivity, or specific heat capacity, needed for temperature calculation, are stored. Currently considered material classes are street, grass, soil, water, building roof, building wall, vegetation.

2.2 Overview of Thermal Simulation

The starting point of our proposed thermal simulation framework is given by the 3D semantic city model, i.e. the three-dimensional triangular mesh with distinct numeric class labels per triangle, as described in Sec. 2.1. Environmental data needed for the simulation, including wind speed, air temperature, or relative humidity, is considered to be available via weather stations nearby the city to be simulated. Due to thermal inertia, a minimum time-span of 48h has to be simulated, such that corresponding weather data has to be gathered. Generally, we calculate the surface temperatures based on the well-known heat equation applied to the full scene. To do so, a finite volume method (FVM) is deployed by expanding each surface triangle of the 3D mesh into a prism of material-dependent depth which is sliced into several layers following (Kottler et al., 2019). Here and in the following, we will refer to this as the surface volume.

For each layer, average temperatures are estimated by modeling the net heat flux. Thus, the surface layer is affected by convective, radiative and conductive heat, while the inner layers only experience heat conduction. Due to its high complexity, latent heat is not yet regarded in the presented work. Following (Kottler et al., 2019; Bartos and Stein, 2015), the temporal temperature evolution for each surface layer is given by

$$\rho_s c_{v,s} d \frac{\partial T_s}{\partial t} = q_{\text{conv}} + q_{s,\text{cond}} + \gamma_{\text{sky}} q_{\text{rad}} + \gamma_{\text{sun}} q_{\text{sol}} \quad (1)$$

with the temperature of the surface T_s , the solar short-

wave heat flux q_{sol} , the radiative long-wave heat flux q_{rad} , the factors $\gamma_{\text{sun}} \in [0; 1]$ yielding whether the surface layer is exposed to sunlight and $\gamma_{\text{sky}} \in [0; 1]$ yielding the relative exposure to the sky in orthogonal direction, the conductive heat flux q_{cond} , the convective heat flux q_{conv} , the material-dependent specific heat capacity $c_{v,s}$ and material density ρ_s of the surface layer, and finally its depth d . The inner layers, i.e. below the surface, only experience conductive heat transfer, yielding

$$\rho_i c_{v,i} d \frac{\partial T_i}{\partial t} = q_{i,\text{cond}} \quad (2)$$

where i indicates the i -th layer with corresponding heat flux $q_{i,\text{cond}}$ and temperature T_i , and it is $i = 1 \dots (n-1)$ with n being the number of layers. The layer depths are assumed to be equal. Depending on the present semantic class and material of the surface element, we set the temperature of the last layer to a constant, or assume the heat flux to be zero, i.e. some kind of insulation being apparent in the semantic object. In the following, details on the heat flux terms will be outlined.

2.3 Conductive Heat

The individual layers of a given surface volume are assumed to exchange heat by conduction following Fourier's law. Furthermore, we assume a lateral heat exchange between surface volumes, in particular between neighboring layers, see Figure 1.

Thus the conductive fluxes in Eq. (1) and ((2)) are

$$q_{s,\text{cond}} = \frac{k_s}{d} (T_1 - T_s) + \frac{d}{A} \sum_{j \in \mathcal{N}_s} k_{sj} (\nabla T)_{sj} \vec{n}_{sj} L_{sj} \quad (3)$$

$$q_{i,\text{cond}} = \frac{k_{i-}}{d} (T_{i-1} - T_i) + \frac{k_{i+}}{d} (T_{i+1} - T_i) + \frac{d}{A} \sum_{j \in \mathcal{N}_i} k_{ij} (\nabla T)_{ij} \vec{n}_{sj} L_{sj} \quad (4)$$

with the area A of the surface triangle, its set of neighboring triangles \mathcal{N}_s , and the length L_{sj} and normal \vec{n}_{sj} of the corresponding edge between the surface and the neighboring triangle indexed by j . It is $\vec{n}_{ij} = \vec{n}_{sj}$ and $L_{ij} = L_{sj}$ for all sub-surface layers i . Hence, $(\nabla T)_{ij}$ denotes the derivative in direction of \vec{n}_{sj} . The conductivity at layer interfaces, denoted by $k_{i\pm}$ and k_{ij} , are determined as $\min(k_i, k_{i\pm 1})$ and $\min(k_i, k_j)$, respectively. As previously stated, we set the boundary conditions on the last layer denoted by n depending on the surface triangles' semantic class, i.e.

$$\begin{cases} (\nabla T)_n = 0 & \text{if building roof or wall} \\ T_n = \text{const.} & \text{otherwise} \end{cases} \quad (5)$$

where $(\nabla T)_n$ denotes the derivative of T along the surface normal.

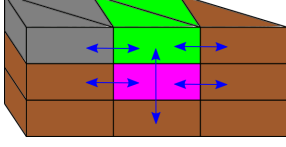


Figure 1: 3D surface volumes. Colors indicate the material classes street (gray), gras (green), soil (brown), and user-defined (magenta). Blue arrays indicate direction of conductive heat transfer.

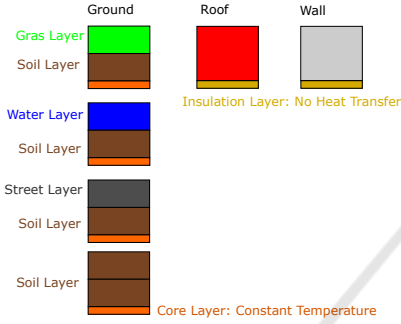


Figure 2: Schematic representation of the material composition per surface class.

Given the numeric semantic class label of the surface triangles, material properties being needed in above equations are deduced. Namely, these are density, specific heat capacity, and heat conductivity. The class label serves as unique identifier referencing to the material library holding these parameters. However, since only the surface class is known, sub-surface materials have to be approximated. The authors of (Kottler et al., 2019) applied the properties of the surface triangle also on sub-surface layers, while commercial software tools such as Envi-met (Liu et al., 2021) provide more sophisticated default compositions of material layers. Yet, case studies using microclimate simulation software often reveal the need for manual adaption of materials to make them a better fit to reality. In our model, we thus provide default as well as adaptable 1D surface volumes. These are defined as an array of materials each with corresponding depth boundaries. The materials are uniquely identified by a numerical value, referencing again the given material library. By default, given the unique surface materials of a semantic 3D city model, the 1D surface volumes are automatically generated and, according to the first material in the array, i.e. the surface material, assigned to the corresponding triangle of the 3D city model. Alternatively, a semi-automatic process can be employed,

where 1D surface volumes are manually defined and automatically assigned to the 3D city model. Figure 1 illustrates the 3D surface volume with directions of heat conduction, and Figure 2 displays the boundary conditions and materials assigned by default to the 1D surface volume.

2.4 Convective Heat

Convection describes the transfer of heat by a moving fluid, such as air or water, and distinction is made between natural convection, where a fluid starts moving due to a change in temperature, and forced convection, where a temperature change occurs due to forced fluid motion by an external source, e.g. wind or ventilators. In an outdoor scene, an example for natural convection is the visible rising air directly above hot streets during summer heat periods. Yet, natural convection often is exceeded by forced convection due to wind movement. Generally, the convective heat flux is proportional to the temperature difference of a given surface and the moving fluid. Introducing the convective heat transfer coefficient (CHTC), the convective heat flux in Eq. (1) is given by

$$q_{s,\text{conv}} = h(T_{\text{air}} - T_s) \quad (6)$$

with the CHTC h . Generally, the estimation of h is a tremendously challenging task. Particularly within a city, dependencies on cityscape, material properties such as roughness or coating, wind speed and many others occur. Corresponding research usually focuses on very specific situations under well-defined conditions. For this reason, we chose a CHTC model that takes into account the 3D geometry of the city model and is based on CFD simulations following (Awol et al., 2020). Therein, the authors propose three new correlations which set into relation the wind speed at 10m height above ground, the building packing density, and the flow regime. The authors differentiate between the isolated (large distance between buildings compared to their height) and interference/skimming (medium to low distance between buildings compared to their height) regimes. They further assume ideal cubic buildings uniformly spread on an orthogonal grid. The proposed correlations from (Awol et al., 2020) are given in the form of

$$h = c_1 \cdot v_{10}^{c_2} \cdot (c_3 \cdot \lambda^2 - c_4 \cdot \lambda + 1) \quad (7)$$

in the isolated flow regime and

$$h = c_1 \cdot v_{10}^{c_2} \cdot (c_5 - c_6 \cdot \lambda) \quad (8)$$

in the interference/skimming flow regime, with the wind speed at 10m height above ground v_{10} and the packing density λ of the buildings. The parameters c_1 ,

$c_2, c_3, c_4, c_5,$ and c_6 depend on the relative surface orientations clustered in the four categories windward, top, lateral and leeward. To apply the proposed correlation to our case, a triangle-wise estimation of the building packing density, the flow regime, and the relative surface orientation category has to be carried out. We hold on to the assumption of cubic buildings and thus estimate the building packing density as

$$\lambda = \frac{A_b}{A_g} \quad (9)$$

with A_b the summarized planar area of all buildings in the scene and A_g the not built-up area, yet involving all ground surfaces, including streets or pavement. The planar areas A_b and A_g are yielded by the orthogonal projection of the 3D city model with its semantic class labels. We further estimate the flow regime by the percentage of the built-up area with respect to the full scene and neglect differences in building heights. Given the LOD1 buildings, each roof triangle is assigned the category *top* of the relative surface orientation. By taking the dot product of surface normals and wind direction, which is assumed to be constant in space and time, wall triangles are assigned the corresponding categories *windward*, *lateral*, or *leeward*. Since the correlations given by Eq. (7) and (8) are only valid for buildings, another CHTC model has to be used for ground and vegetation. At ground, parallel laminar flow is assumed, and from (Energie und Umwelttechnik, 2009), we formally set the CHTC to

$$h = \begin{cases} 7.3v_{10}^{0.73}, & \text{if } v_{10} > 5 \text{ m/s} \\ 1.8 + 4.1v_{10}, & \text{otherwise} \end{cases} \quad (10)$$

depending on the wind speed, i.e. whether forced convection outperforms natural convection or not.

The CHTC model above is valid for building triangles, yet ground and vegetation triangles have to be considered separately. Vegetation further raises the challenge in thermal modeling due to their active nature, as it actively regulates its temperature via evapotranspiration to a certain degree (Kibler et al., 2023). In our approach, we assume the temperature of vegetation to be equal to air temperature. Thus, latent heat accounting for the effect of transpiration and evaporation from vegetation as well as moist ground is not included in our model for the sake of simplicity.

2.5 Radiative Heat

Radiative heat exchange in an urban area can be separated in heating due to solar exposure, heat exchange between objects, and exchange between surfaces and the surrounding atmosphere. While the first particularly occurs due to the short-wave infrared radiation within the solar spectrum, the latter two occur

in the long-wave infrared spectrum, which is also known as thermal radiation and strongly depends on the scenery, namely the surface materials, surface areas and their mutual exposure.

We formally follow (Kottler et al., 2019; Bulatov et al., 2020) to model both radiative heat fluxes. Thus, the solar heat flux q_{sol} on an exposed surface oriented by the angle ϕ in direction of the incoming sunlight is given by

$$q_{\text{sol}} = (1 - a)E_s \cos(\phi) \quad (11)$$

with the color-dependent solar albedo a , i.e. the solar reflectance of the surface, and the solar irradiation E_s at the surface, i.e. damped by the atmosphere. The sky is mathematically assumed as infinite surface with a corresponding sky temperature T_{sky} yielding the long-wave radiative heat flux

$$q_{\text{rad}} = \sigma \varepsilon (T_{\text{sky}}^4 - T_s^4) \quad (12)$$

with the emissivity ε of the surface material and the Stefan-Boltzmann constant σ .

2.6 Initial Condition

The numerical estimation of temperatures in transient heat transfer states an initial value problem and due to thermal inertia, the initial temperature distribution is crucial and affects the temporal temperature evolution. This is why the simulation of temperatures of a 3D city model at a given point in time should always include the simulation of temperatures for a preceding time span, from a few hours up to a few days depending on the chosen initial temperatures. When measured temperature distributions are given, the preceding simulation time can be minimized. Our overall simulation framework was thus designed to allow for aerial thermal imagery to be used as initial data, whereas unseen structures are interpolated. For example, these might be walls, windows, or tree trunks. If no measured data is available, a 1D precalculation, i.e. no lateral heat conduction, of material-wise temperatures is performed. In other words, the 1D temperature distribution of each unique surface volume is independently simulated. Each surface volume is assumed to represent a flat triangle with no elevation nor shadowing, the environmental conditions are given by the first 24 hours of the overall timespan to be simulated, and the first air temperature entry serves as initial temperature.

2.7 Thermal Radiance for Image-to-Image Comparison

Generally, when an aerial thermal image is provided, measured surface temperatures need to be deduced.

Since any thermal camera generally measures heat radiance instead of actual temperatures, the camera sensor output is translated into temperature values by some approximations either within the camera or by camera-specific tools. Yet, the underlying correlations, applied approximations and specifications are usually company property, thus not publicly available and often not provided. To compare the simulated surface temperatures against thermal imagery, we thus consider not only the simulated surface temperatures themselves but also the simulated heat radiance for better image-to-image comparability. Given the simulated surface temperatures T_s , this radiance is approximated by

$$L = \epsilon \int_{\lambda_1}^{\lambda_2} L_\lambda(\lambda, T_s) d\lambda \quad \text{whereby} \quad (13)$$

$$L_\lambda(\lambda, T) = \frac{c_1}{\lambda^5} \cdot \left(\exp\left(\frac{c_2}{\lambda \cdot T_s}\right) - 1 \right)^{-1}$$

with the material-wise thermal emissivity ϵ , integration over the long-wave infrared spectrum with $\lambda_1 = 8\mu\text{m}$ and $\lambda_2 = 14\mu\text{m}$, and the spectral radiance following Planck's law with constants c_1 and c_2 . The integral can be solved numerically by transforming into a fast converging series, yielding (Wallrabe, 2001)

$$L = \epsilon \frac{c_1 T^4}{c_2^4} [S(x_1) - S(x_2)] \quad \text{whereby} \quad (14)$$

$$S(x_n) = \sum_{i=1}^{\infty} \frac{(ix_n)^3 + 3(ix_n)^2 + 6ix_n + 6}{i^4 \exp(ix_n)}$$

with $x_n = \frac{c_2}{\lambda_n T_s}$ for $n = 1, 2$.

To keep the radiance model as simple as possible, atmospheric or sensor-specific effects are not modeled. With simulated temperature and radiance values per triangle, a simple OpenGL rendering is performed in order to generate simulated images of the area in correspondence to the measured thermal image.

3 RESULTS

The simulation approach has been carried out for an urban area in the City of Melville, Western Australia. The reconstructed area of size $2 \text{ km} \times 1 \text{ km}$ is shown in Figure 3. The reconstruction as discussed in Sec. 2.1 is a triangle mesh with semantics and materials assigned. This mesh consists of 1648685 triangles. Hereby, buildings are given with level-of-detail (LOD) 1 while the vegetation is represented either as a standard tree model for isolated single trees and shrubs or as forest boxes for larger tree regions. Environmental conditions for the simulation are drawn from a nearby weather server.

Figure 4 shows an excerpts of the simulation results. As the temperature is calculated per triangle, the triangle mesh with the corresponding temperatures given at 8pm is shown (top image). The two bottom images show the results of the urban area at 8pm from different viewpoints, showing the impact of the 3D characteristics taken into account, i.e. the wall temperatures differ according to their relative orientation (north/south, east/west).

3.1 Qualitive Evaluation of the Initial Condition

An aerial thermal image of the considered area was provided, such that both initial condition implementations are tested. Figure 5 displays the initial temperatures set from the aerial image, and by precalculation, i.e. material-wise approximations. As described in Sec. 2, the precalculation starts with uniform temperature all over the scene equal to air temperature, and the calculated initial temperatures already reveal the diverse material characteristics in the urban area. Street and ground becomes distinguishable from vegetation and buildings. Furthermore, while street and soil are comparable to the thermal image temperatures, grass temperatures appear overestimated, and vegetation and building temperatures tend to underestimation. The precalculated values still suffer from said starting values, i.e. air temperature, and more detailed evaluation will be considered from the final simulation results in the following.

3.2 Evaluation of Simulation Results

The evaluation is based on two components. First, image similarity measures are considered since an aerial image is given as ground truth data. To quantify image similarity from both human perception and from a computer vision point of view, the metrics of mutual information (MI) and structural similarity index measure (SSIM) are employed. MI originally stems from information theory and quantifies the statistical correlation between two variables. SSIM quantifies the similarities of two images by their luminance, contrast and structure. Second, given the measured surface temperatures from the thermal image and simulated surface temperatures, the root-mean square error (RMSE) and mean absolute error (MAE) of the simulation are considered as well. Besides taking into account the fully rendered area, RMSE and MAE are also evaluated in a class-wise manner to assess the class-specific modeling of heat conduction.

As described in Sec. 2.7, an orthogonal projection of the 3D triangle mesh with surface temperatures

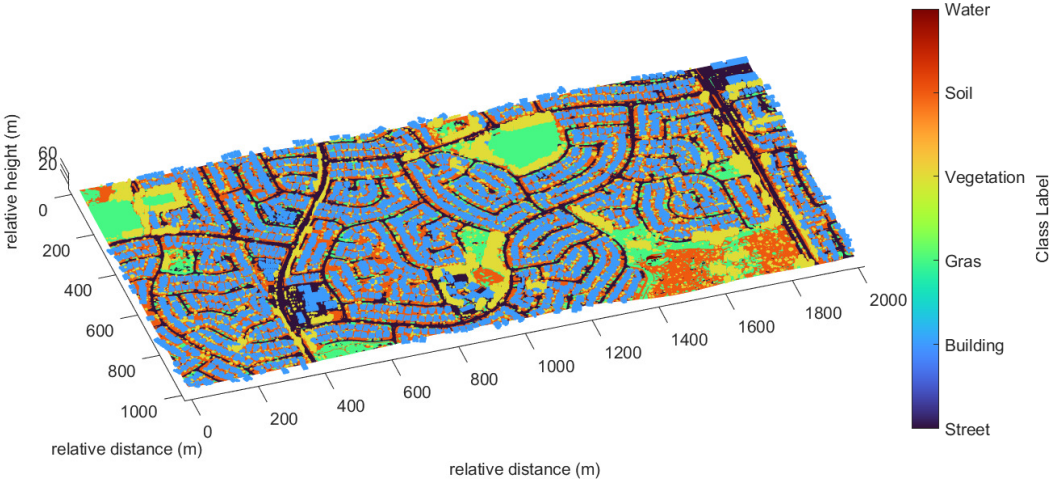


Figure 3: Reconstructed area as triangle mesh with respective class labels.

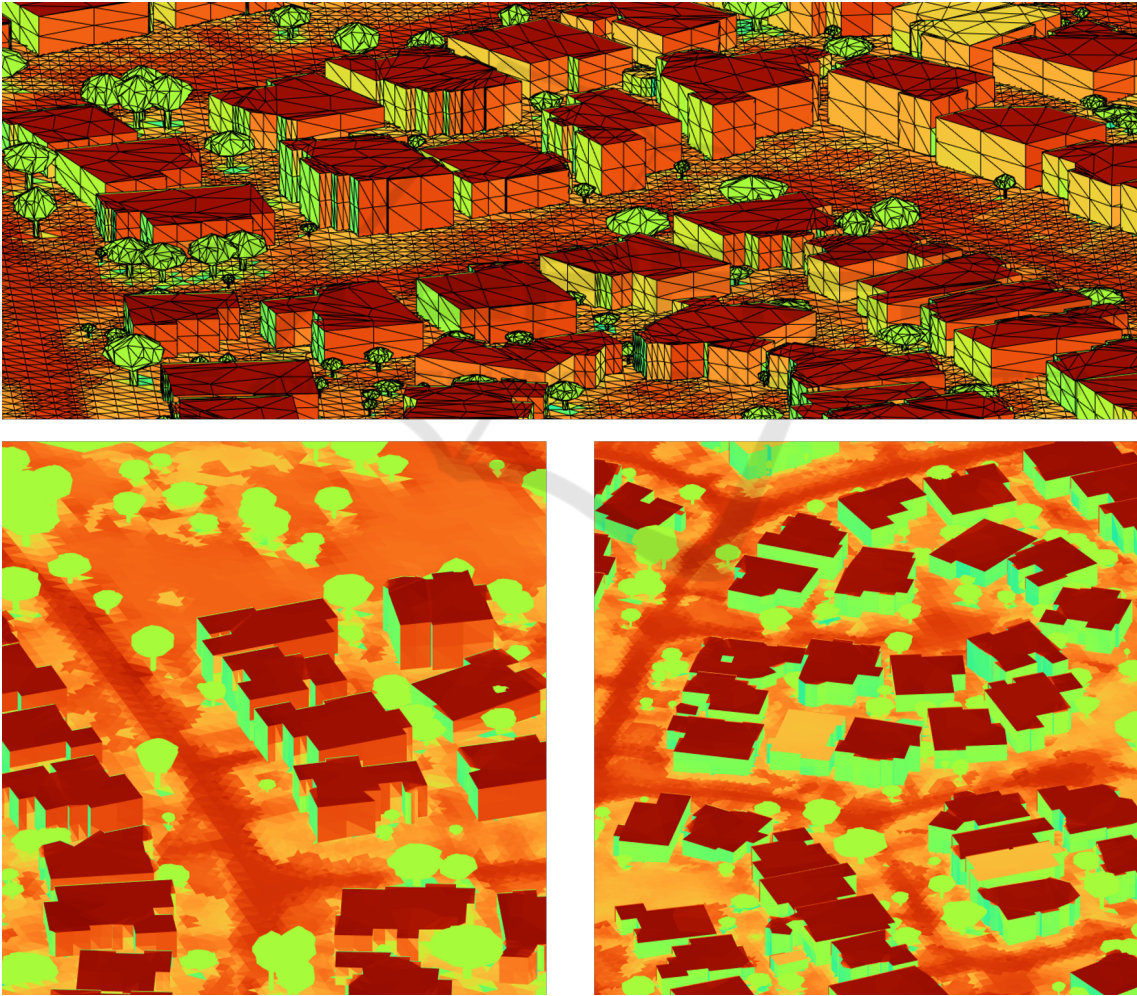


Figure 4: Qualitative results of the heat simulation on the LOD1 reconstruction of the urban area at 8pm. Top: simulated surface temperatures displayed together with the triangle mesh. Bottom: simulated surface temperatures displayed without triangle mesh. Left: view from the west. Right: view from the east.

Table 1: Image similarity by mutual information (MI) and structural similarity index measure (SSIM).

Initial Condition	Rendered Value	MI	SSIM
Precalculated	Temperature	0.61	0.50
	Long-Wave IR Radiance	0.60	0.63
Thermal Image	Temperature	1.19	0.67
	Long-Wave IR Radiance	1.00	0.67

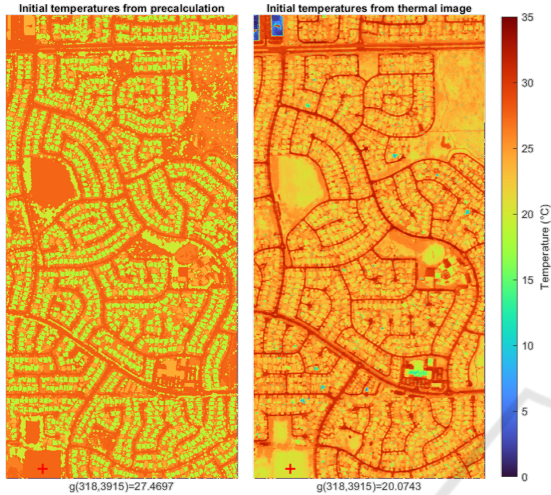


Figure 5: Initial temperatures from precalculation (left), i.e. material-dependent temperature value, and initial temperatures from a given thermal image (right).

Table 2: Root-Mean-Square-Error (RMSE) and Mean Average Error (MAE) of simulated temperature values over all classes, i.e. considering the full scene, and class-wise only.

Initial Condition	Class	RMSE	MAE
Precalculated	All	8.56	6.96
	Street	4.31	0.62
	Soil	3.96	1.12
	Gras	10.23	1.25
	Buildings	13.58	12.96
	Vegetation	5.52	5.40
Thermal Image	All	8.28	6.64
	Street	4.34	0.73
	Soil	2.98	0.89
	Gras	7.85	0.97
	Buildings	13.97	13.26
	Vegetation	5.52	5.40

and radiances is applied. The resulting images, together with the measured aerial image, are displayed in Figure 6. There, the effect of emissivity, i.e. the material-dependent ability of surfaces to radiate heat, can clearly be seen in the simulated long-wave infrared image. Simulation of the surface temperatures took approximately 2 hours (application of initial temperatures excluded) on a personal computer (Intel(R) Core(TM) i9-10900K, CPU@3.70GHz, 32GB RAM, Nvidia GeForce RTX 2080 Super) and the

Matlab Parallelization Toolbox was used for GPU usage. Please note that the implementation of the mathematical model was conducted under the premise of prototyping a simulation framework in an object-orienting programming (OOP) matter in MATLAB 2021 and is not runtime-optimized. Therefore, absolute run-times of the overall simulation are not representative since OOP does not perform fast in MATLAB, however, the final coding structure of our implementation is easily transferable to other programming languages, allowing the fast implementation of plugins for software in the field of 3D graphics or virtual environments.

As first part of the evaluation, image similarity is considered, and MI and SSIM are summarized in Table 1. By determining the initial temperatures by the given thermal image, MI is strongly increased. This is expected and likely caused by the inner-class temperature variations introduced by the initial temperatures. Yet, MI is reduced when long-wave infrared radiance is compared to the measured thermal image. Two potential causes occur: first, the radiance model might be oversimplified. Second, the processing of the thermal image before delivery causes unexpected and undocumented deviations. The SSIM shows generally good agreement between measurement and simulation, yet, usage of long-wave infrared radiance instead of surface temperatures shows none or only minor improvement, presumably for the same reasons as stated above.

As second part of the evaluation, RMSE and MAE of the simulated surface temperatures are determined against the measured temperatures from the thermal image, as previously outlined, and summarized in Table 2. With an MAE of 6.96 for precalculated initial values and 6.64 when the thermal image is applied as initial condition, the need for a class-wise consideration is raised. There, ground classes (street, soil, gras) show good agreement with the measurements, however, buildings and vegetation deviate, increasing the comprehensive MAE. With vegetation being challenging to model due to its active nature, and given the applied simplified model, a larger deviation than other classes was expected. The high MAE value on buildings lies in an overestimation of roof temperatures, cp. Figure 6, originating most likely from an underestimation of weather conditions and heavy generaliza-

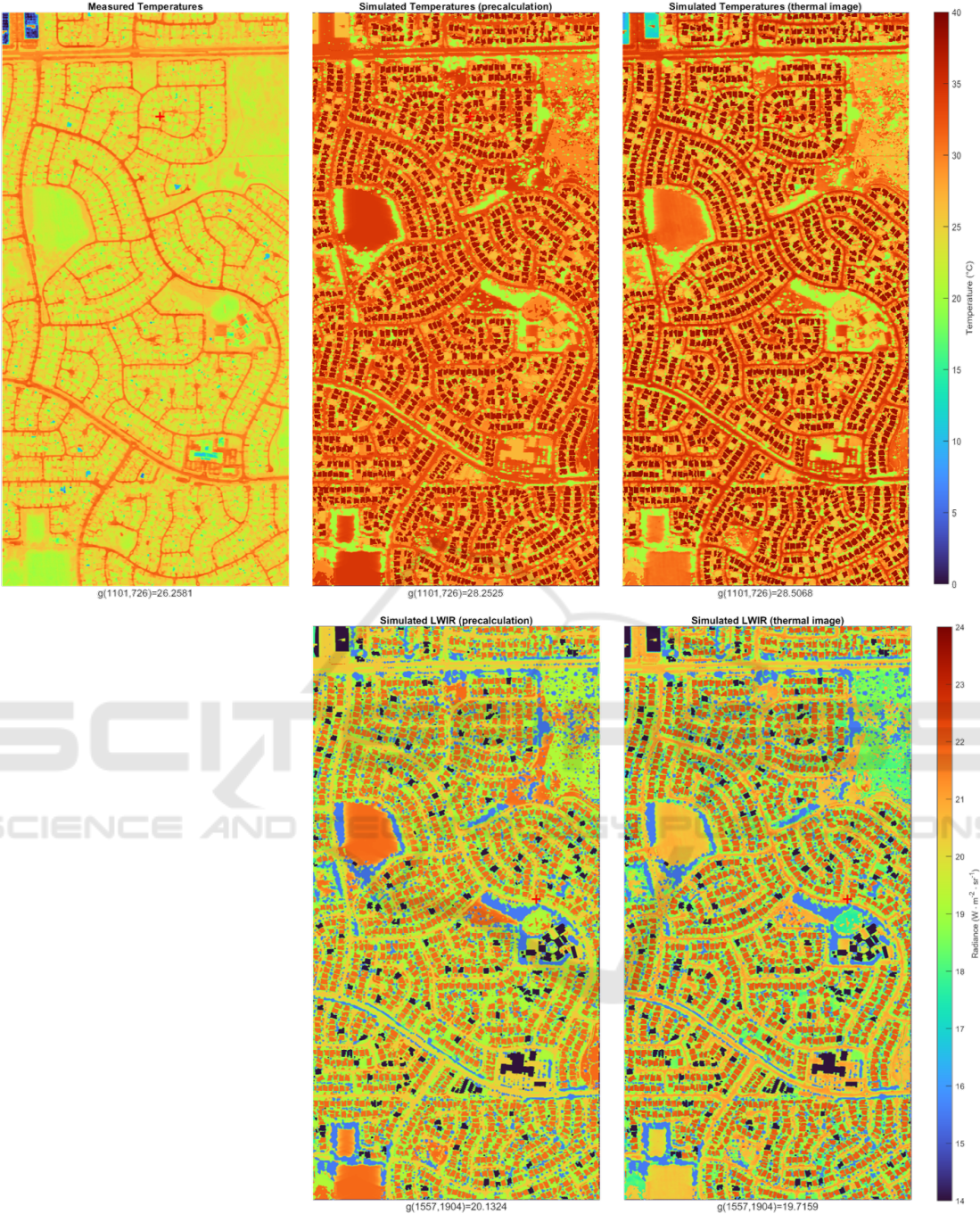


Figure 6: Measured and simulated thermal images. From left to right: measured temperatures from aerial thermal image, simulated surface temperatures with initial temperatures from precalculation (top) with corresponding simulated long-wave infrared radiance image (bottom), and simulated temperatures with initial temperatures from thermal image (top) with corresponding simulated long-wave infrared radiance image (bottom).

tions in roof construction. The underlying roof model including insulation is generalized to most cities, yet in our test area, i.e. the City of Melville, insulation is often missing. Indeed, many buildings even allow for air circulation between building walls and roof.

Comparing the initial conditions, only slightly better results are found when the thermal image is used. The precalculation is supposed to overcome the thermal inertia rendering the initial condition crucial, thus this minor improvement aligns with expected behavior. From the class-wise approach, ground surfaces suffer from outliers with large deviations between simulation and measurement. A reasonable explanation are the neglected variations in moist, soil composition, and street types (e.g. asphalt, concrete, pavement).

In summary, the simulation shows good agreement with the measured temperatures for most classes, yet buildings and vegetation will need further improvement in future work.

4 CONCLUSION

We presented a tool for temperature computation of urban areas being more precise in thermal modeling than game-oriented software yet less computationally heavy than microclimate simulations. Starting at meshes derived from multi-source sensor data, we are driven by the motivation to create realistic temperature values which will allow for faster decisions in urban planning.

We realized that the path from raw multi-source sensor data to thermal image of an urban area is challenging and complex. The geo-referenced 3D parametric model, enriched with the weather data, makes it possible to derive the temperatures of the scene elements at any moment of time, and from there, the radiance (infrared) image can be generated. The negative consequence of a complex procedure is always that an inaccuracy at a very early stage results in barely inexplicable deviation from the reference data in the final output. Providing a better co-registration of sensor data; more robust procedures for land cover and material classification; higher levels of details for buildings and trees; consideration of further terms for infrared image synthesis out of surface temperatures: all this influences the quantitative result greatly. In this work, we concentrated on the underlying physics-based thermal models. Semantic- and material-dependent models for conductive and convective heat were presented. There, the convective model by (Awol et al., 2020) has been adapted to real urban areas. To handle the thermal inertia and the

challenging initial temperature conditions, material-wise precalculation and usage of thermal imagery were introduced, and the precalculation show promising results which is of importance as acquisition of thermal imagery can be challenging.

In summary, our approach yielded promising results for a quick, superficial screening of a large urban scene. Such a quick screening can assist in urban planning. Yet, the simplified vegetation model of the simulator at its current stage is a major drawback. Improving this model, by integrating latent heat, is one important direction of future work. Furthermore, we strive for the inclusion of a simplified CFD simulation, i.e. replacing the global wind velocity and direction by triangle-wise values. Naturally, as the current implementation is in form of a prototype, we furthermore strive for a final implementation and comparison of absolute runtimes to microclimate simulation and gaming approaches.

ACKNOWLEDGEMENTS

Many thanks for providing the multi-source data of the test site, City of Melville, particularly to Dr. Petra Helmholtz from Curtin University, Australia.

REFERENCES

- Awol, A., Bitsuamlak, G. T., and Tariku, F. (2020). Numerical estimation of the external convective heat transfer coefficient for buildings in an urban-like setting. *Building and Environment*, 169:106557.
- Bartos, B. and Stein, K. (2015). FTOM-2D: a two-dimensional approach to model the detailed thermal behavior of nonplanar surfaces. In Stein, K. U. and Schleijsen, R. H. M. A., editors, *Target and Background Signatures*, SPIE Proceedings, page 96530G. SPIE.
- Bulatov, D., Burkard, E., Iehag, R., Kottler, B., and Helmholtz, P. (2020). From multi-sensor aerial data to thermal and infrared simulation of semantic 3D models: Towards identification of urban heat islands. *Infrared Physics & Technology*, 105:103233.
- Energie und Umwelttechnik (2009). Wärme- und Kälteschutz von betriebstechnischen Anlagen in der Industrie und in der technischen Gebäudeausrüstung - Berechnungsgrundlagen [Thermal insulation of heated and refrigerated operational installations in the industry and the building services - calculation rules]. Technical Report VDI 2055 Blatt 1, VDI Verein Deutscher Ingenieure e.V.
- Kibler, C. L., Trugman, A. T., Roberts, D. A., Still, C. J., Scott, R. L., Caylor, K. K., Stella, J. C., and Singer, M. B. (2023). Evapotranspiration regulates leaf tem-

- perature and respiration in dryland vegetation. *Agricultural and Forest Meteorology*, 339:109560.
- Kottler, B., Burkard, E., Bulatov, D., and Haraké, L. (2019). Physically-based thermal simulation of large scenes for infrared imaging. In *VISIGRAPP (1: GRAPP)*, pages 53–64.
- Liu, Z., Cheng, W., Jim, C. Y., Morakinyo, T. E., Shi, Y., and Ng, E. (2021). Heat mitigation benefits of urban green and blue infrastructures: A systematic review of modeling techniques, validation and scenario simulation in ENVI-met V4. *Building and Environment*, 200:107939.
- Oktal-SE (2023). Oktal Synthetic Environment. <http://www.oktal-se.fr/website/>. Accessed: 2023-10-26.
- Presagis (2023). Presagis Canada Inc. <https://www.presagis.com/en/>. Accessed: 2023-10-26.
- Rodríguez-Vázquez, Martin and Hernández-Pérez, Iván and Xamán, Jesus and Chávez, Yvonne and Gijón-Rivera, Miguel and Belman-Flores, Juan M. (2020). Coupling building energy simulation and computational fluid dynamics: An overview. *Journal of Building Physics*, 44(2):137–180.
- Ruijun Zhang, P. A. M. (2021). Cfd-cfd coupling: A novel method to develop a fast urban microclimate model. *Journal of Building Physics*, 44(5):385–408.
- Wallrabe, A. (2001). *Nachtsichttechnik: Infrarot-Sensorik: physikalische Grundlagen, Aufbau, Konstruktion und Anwendung von Wärmebildgeräten [Low-light-level technology: Infrared Sensor Technology: physical basics, structure, construction and application of thermal imaging devices]*. Springer, Braunschweig/Wiesbaden, 1st edition.